PREDICTION OF LIFT LOSSES DUE TO SURFACE ROUGHNESS BY MEANS OF A 2D NAVIER-STOKES SOLVER

Per Weinerfelt
SAAB Aerospace, Sweden

Keywords: *surface roughness, Navier-Stokes calculations*

Abstract

The 2D Navier-Stokes code ns2d at SAAB Aerospace has been used to simulate the effect of surface roughness for several 2D flow cases and geometries. The effect of surface roughness has been modelled by a modification of the wall distance in the Chien's $\kappa - \varepsilon$ *model. The flow over a flat plate, the NACA* $65_2 - A2155$ *wing profile and the SAAB 2000 wing/flap geometry, for both clean and rough surfaces, have been computed. Comparisons with wind tunnel/flight test data are also presented.*

1 Introduction

An important issue for an aircraft industry is to predict correctly how ice or de-icing fluids effect the lift characteristics of the aircraft. Experiments and flight tests are expensive and in some situations impossible to carry out. CFD programs and the computers have on the other hand become better and cheaper and hence a reliable alternative. The present paper describes how the 2D Navier-Stokes code ns2d at SAAB Aerospace has been used to simulate the effect of surface roughness for several 2D flow cases and geometries. The main objective of this work is to estimate the losses in c_l, to be expected shortly after take off, due to remaining de-icing fluid on the wing surfaces.

2 Description of the Navier-Stokes code ns2d

The code ns2d is a two-dimensional time-dependent compressible Reynolds averaged Navier-Stokes solver. The main parts of the solver are presented in the sections below. Section 2.1-2.3 describe the mean flow and the turbulence models used in ns2d. In 2.4 the modelling of surface roughness is discussed. In the last section 2.5 the numerical methods in ns2d are briefly described.

2.1 Reynolds averaged Navier-Stokes equations

Integrating the two-dimensional time-dependent compressible Reynolds averaged Navier-Stokes equations written in conservative form over an arbitrary quadrilateral cell $\Omega_{i,j}$ yields

$$\iint_{\Omega_{i,j}} \frac{\partial W}{\partial t} dx dy + \int_{\partial\Omega_{i,j}} H(W)\, \hat{n}\, ds = 0$$

where $\hat{n}$ is a unit vector normal to the boundary and $W = (\rho, \rho U_1, \rho U_2, \rho E)$ a vector of conserved variables. The components of W are the Reynolds averaged density ρ, the Favre averaged velocity components U_1, U_2 in the Cartesian coordinate direction x_1, x_2 and the Favre averaged total energy per unit mass E. The flux tensor H is decomposed into a convective and viscous/turbulent part
$H = (F^c - F^{v,t}, G^c - G^{v,t})$. The convective fluxes are given by

$$F^c = \begin{pmatrix} \rho U_1 \\ \rho U_1^2 + p \\ \rho U_1 U_2 \\ (\rho E + p) U_1 \end{pmatrix}, \; G^c = \begin{pmatrix} \rho U_2 \\ \rho U_1 U_2 \\ \rho U_2^2 + p \\ (\rho E + p) U_2 \end{pmatrix}$$

where p is the Reynolds averaged static pressure. For the viscous and turbulent fluxes we have

$$F^{v,t} = \begin{pmatrix} 0 \\ \tau_{11} - \overline{\rho u_1^2} \\ \tau_{12} - \overline{\rho u_1 u_2} \\ U_1 \left(\tau_{11} - \overline{\rho u_1^2}\right) + U_2 \left(\tau_{12} - \overline{\rho u_1 u_2}\right) - q_1 \end{pmatrix}$$

$$G^{v,t} = \begin{pmatrix} 0 \\ \tau_{12} - \overline{\rho u_1 u_2} \\ \tau_{22} - \overline{\rho u_2^2} \\ U_1 \left(\tau_{12} - \overline{\rho u_1 u_2}\right) + U_2 \left(\tau_{22} - \overline{\rho u_2^2}\right) - q_2 \end{pmatrix}$$

The notation $\overline{\phi}$ stands for the Reynolds average of ϕ and u_i is the velocity deviation from the mean velocity U_i. For a Newtonian fluid the components of the stress tensor τ can be expressed in terms of the mean velocity gradients and the viscosity coefficient μ according to

$$\tau_{ij} = \mu \left(\frac{\partial U_i}{\partial x_j} + \frac{\partial U_j}{\partial x_i} - \frac{2}{3} \delta_{ij} \frac{\partial U_m}{\partial x_m} \right)$$

Applying the Boussinesq eddy viscosity concept the Reynolds stresses $\overline{\rho u_i u_j}$ and the heat fluxes q_i can be formulated as

$$\overline{\rho u_i u_j} = -\mu_t \left(\frac{\partial U_i}{\partial x_j} + \frac{\partial U_j}{\partial x_i} - \frac{2}{3} \delta_{ij} \frac{\partial U_m}{\partial x_m} \right) + \frac{2}{3} \delta_{ij} \rho \kappa$$

$$q_i = -C_p \left(\frac{\mu}{Pr} + \frac{\mu_t}{Pr_t} \right) \frac{\partial T}{\partial x_i}$$

where T is the temperature, μ_t is the turbulent viscosity and κ the turbulent kinetic energy. The Prandtl numbers Pr and Pr_t are chosen as $Pr = 0.72$ for laminar and $Pr_t = 0.90$ for turbulent flows. Finally the perfect gas law couples the pressure and temperature to the conserved variables

$$p = T\rho \;\text{ and }\; T = (\gamma - 1) \left(E - \frac{1}{2} \left(U^2 + V^2 \right) - \kappa \right)$$

2.2 Turbulence Transport Equations

In order to close the system above some additional equations, including κ and μ_t, have to be introduced. The turbulent kinetic energy and its dissipation rate ε are computed from the transport equations

$$\begin{aligned} \frac{\partial}{\partial x_j} (\rho U_j \kappa) &= \frac{\partial}{\partial x_j} \left(\left(\mu + \frac{\mu_t}{\sigma_\kappa} \right) \frac{\partial \kappa}{\partial x_j} \right) + P_k - \rho \varepsilon \\ \frac{\partial}{\partial x_j} (\rho U_j \varepsilon) &= \frac{\partial}{\partial x_j} \left(\left(\mu + \frac{\mu_t}{\sigma_\varepsilon} \right) \frac{\partial \varepsilon}{\partial x_j} \right) + \\ & \quad c_{1\varepsilon} \frac{\varepsilon}{\kappa} P_k - c_{2\varepsilon} \frac{\rho \varepsilon^2}{\kappa} \end{aligned} \tag{1}$$

The production term P_k is defined as

$$P_k = -\overline{\rho u_i u_j} \frac{\partial U_i}{\partial x_j}$$

and the turbulent viscosity μ_t is obtained from κ and ε as $\mu_t = c_\mu \frac{\rho \kappa^2}{\varepsilon}$. The constants in (1) have the following values $\sigma_\kappa = 1.0$, $\sigma_\varepsilon = 1.3$, $\sigma_\mu = 0.09$, $\sigma_{1\varepsilon} = 1.44$ and $\sigma_{2\varepsilon} = 1.92$. The present turbulence model is called the standard high-Reynolds Jones-Launder $\kappa - \varepsilon$ model.

2.3 Near Wall Modelling

The κ-ε equations do not account for the interaction between turbulence and fluid viscosity and do not therefore apply to the semi-viscous near wall region. We have in the present paper used the Chien low-Reynolds $\kappa - \varepsilon$ model in [4] near walls. In the Chien model damping functions and additional source terms are added in order to account for viscous effects close to a wall. The source terms are given by

$$S_\kappa = 2\mu \frac{\kappa}{y_n^2} \quad \text{and} \quad S_\varepsilon = 2\mu \frac{\varepsilon}{y_n^2} e^{-y_n^+/2}$$

where $y_n^+ = \frac{\rho y_n u_\tau}{\mu}$, y_n denotes the distance to the wall and u_τ the friction velocity at the wall. A damping function for the turbulent viscosity is introduced according to

$$f_\mu = 1 - e^{-0.0115 y_n^+}$$

The source term $c_{2\varepsilon}\frac{\rho\varepsilon^2}{\kappa}$ is also damped by the function

$$f_2 = 1 - 0.22\, e^{-(R_T/6)^2} \quad \text{where} \quad R_T = \frac{\rho\kappa^2}{\mu\varepsilon}$$

The constants $c_{1\varepsilon}$ and $c_{2\varepsilon}$ are slightly modified $c_{1\varepsilon} = 1.44$ and $c_{2\varepsilon} = 1.92$.

2.4 Surface roughness in the Chien $\kappa - \varepsilon$ model

The effect of surface roughness can be predicted, using the Chien κ-ε model, by simply replacing the wall distance y_n by $y_n + R$. R is a distance computed from the following expressions, originating from Rotta [6]. A similar approach have also been used in [4].

$$\hat{R} = \begin{cases} \sqrt{k_s^+} - k_s^+\, e^{-k_s^+/6}, & 4.5 < k_s^+ \leq 70 \\ 0.7{k_s^+}^{0.58}, & 70 < k_s^+ \leq 2000 \\ 0.031 k_s^+, & k_s^+ > 2000 \end{cases}$$

and $R = \hat{R} \cdot \left(\frac{0.9\mu}{\rho u_\tau}\right)$. Here k_s is an equivalent sand-grain roughness height. The effect of shifting the wall distance by R is that the eddy viscosity is increased in the near-wall region.

2.5 Numerical methods in ns2d

The code ns2d solves the two-dimensional time-dependent compressible Reynolds averaged Navier-Stokes equations written in conservative form. The mean flow equations are discretized in space using a cell-centered finite volume approximation. Central differences are used for the convective fluxes. For the viscous fluxes, the gradients of velocity and temperature are first evaluated on the cell edges. The viscous fluxes are then computed in the same way as the convective fluxes. The molecular viscosity is determined from Sutherland's law.

A blend of second and fourth order adaptive artificial dissipation terms are added to the numerical scheme preventing oscillations in the vicinity of shock-waves and suppressing odd/even decoupling in the solution. In boundary layers the influence of the artificial dissipation can be decreased through a local Mach number scaling.

At solid wall surfaces no-slip and adiabatic wall conditions are used. The far-field boundary conditions are computed from one-dimensional Riemann invariants. In order to allow the far-field boundary to be placed closer to the airfoil, without affecting the accuracy of the solution, a velocity correction, based on the circulation obtained from the computed lift, is applied.

In order to reach a steady state solution the mean flow equations are integrated in time using an explicit five-step Runge-Kutta scheme where the contribution from the dissipation (artificial and physical) is frozen after the second stage. A semi-implicit time marching technique has recently been implemented. The convective and viscous terms are then treated implicitly in the normal wall direction. Local time stepping as well as a FAS multigrid method are available for convergence acceleration.

A number of different turbulence models are available in the code such as the Baldwin-Lomax model and different variants of the $\kappa - \varepsilon$ model. Our base line two equation model is the standard $\kappa - \varepsilon$ model by Jones and Launder. The diffusive terms are discretized using central differences, while for the convective terms a hybrid upwind/central differencing is used. For stability reasons the equations are treated implicitly. In the present work the near wall flow is modelled by the Chien model $\kappa - \varepsilon$.

Transition from laminar to turbulent flow is imposed at the prescribed locations by setting the turbulent viscosity, in the cell layer adjacent to the wall, to 1% of the laminar one in the production term appearing in the κ-equation.

A surface roughness model, described in the previous section, has recently been implemented in ns2d.

3 Results

We will in this section discuss results obtained from flow computations over different 2D ge-

ometries. The flow over both clean and rough surfaces have been studied. In section 3.1 the flow over a flat plate is considered. Section 3.2 focus on the flow over the NACA65$_2$ – A215 wing profile and in 3.3 the effect of leading edge ice and surface roughness on SAAB 2000 wing/flap geometry is investigated. Comparisons with experiments/flight tests are also presented.

3.1 Flat plate

In order to validate the Chien turbulence model and the roughness model in ns2d the flow over a flat plate was computed. For this flow case there exist classical results in the literature both for the smooth and the rough plate. The turbulent flow over a smooth plate, at a free stream Mach number of M_∞ = 0.2 and a Reynolds number of Re = 3.9 million, was first computed. Computed and theoretical velocity profiles are shown in figure 1. The results agree well in both the viscous sublayer and in the logarithmic layer. The skin friction distribution over the smooth plate, $k_s/L = 0$, is found in figure 2. The theoretical results (see [8], p.542-543) are due to Nikuradse (theory 1) and Schulz-Grunow (theory 2). The computed results are close to the two theoretical results as can be seen in figure 2.

For the validation of the roughness model the same flow case was used. Two equivalent sand-grain roughness, $k_s/L = 0.001$ and $k_s/L = 0.002$, were selected. The roughness cover range was 100% of the plate. The theoretical results, denoted by theory 3, are described in [8], p.553. The deviation, displayed in figure 3, between computed and theoretical results are also for this flow case small.

3.2 NACA65$_2$ – A215 airfoil

The airfoil NACA65$_2$ – A215 has been used in the literature for validation of roughness models. There are also experimental results [5] available for this airfoil. The same calculations as in [2] have been done for a free stream Mach number of M_∞=0.182 and a Reynolds number of Re=2.6 million. Calculations for both a smooth and a rough airfoil have been performed. For the

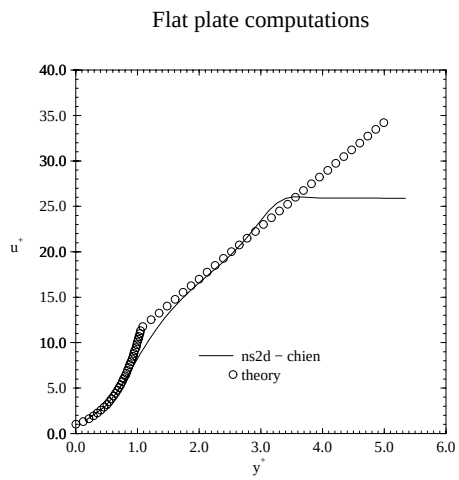

Fig. 1 Computed and theoretical velocity profiles from the flow over a smooth flat plate at M_∞=0.2 and Re=3.9 million.

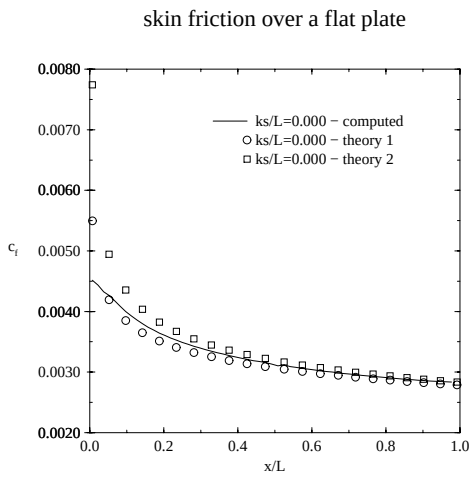

Fig. 2 Computed and theoretical skin friction for the flow over a smooth flat plate at M_∞=0.2 and Re=3.9 million.

roughness calculations, similar to those by Hellsten [2], a roughness parameter of k_s = 0.00123 was selected. The roughness cover range was from 15% on the lower surface to the trailing

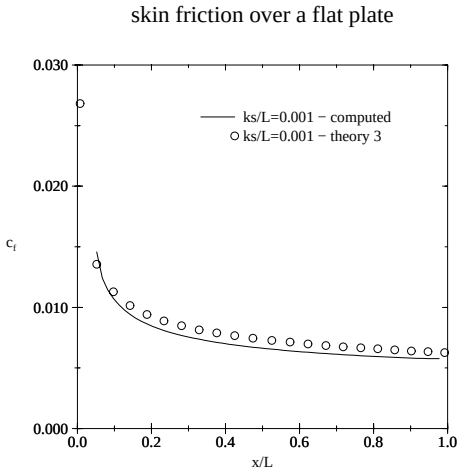

Fig. 3 Computed and theoretical skin friction for the flow over a rough flat plate at M_∞=0.2 and Re=3.9 million. Roughness parameter k_s/L=0.001.

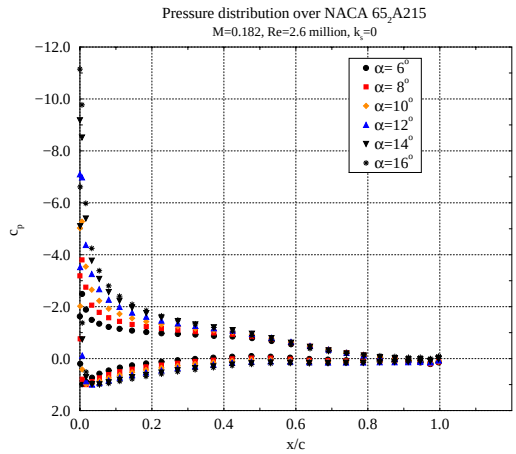

Fig. 4 Pressure distribution, for different angles of attack, over NACA $65_2 - A215$ at M_∞=0.182, Re=2.6 million and k_s=0.

edge on the upper surface which means that the complete upper part of the airfoil, including the leading edge region, was covered. For comparison we have also computed the flow for a smaller cover range starting at 10% of the upper surface ending at the trailing edge. By comparing the results for the two cover ranges an estimate of the effect of a rough leading edge can be obtained. Such a study, for the SAAB 2000 wing/flap geometry, will also be discussed in the next section.

Figure 4 gives an overview of the pressure distribution over the airfoil for $\alpha = 6^o$ up to 16°. From the c_l curve of the smooth airfoil in figure 5 we see that the lift increases from 6° to 16°. The stall occurs close to $18^o - 19^o$. However for the rough airfoil there is a shift in $\alpha_{c_{l,max}}$. For k_s=0.00123 and a cover range starting at 15% of the lower surface the shift is $2^o - 3^o$. The losses in c_l are about 0.30 for this case and 0.20 for the smaller cover range. Hence the leading edge roughness has a non negligible effect on the lift losses. Comparing the results from the present calculations with those obtained by Hellsten we predict a higher $c_{l,max}$ value for both the smooth and the rough airfoil (see figure 6). Lift curves from wind tunnel experiment are shown in the same figure. The discrepancy between these are fairly large indicating mismatching in the experimental setup. However the experiments and the computations predict approximately the same losses in $c_{l,max}$, at $\alpha_{c_{l,max}}$, due to the surface roughness (figure 7).

3.3 SAAB 2000 wing/flap geometry

In this section the results from roughness computations applied to the SAAB 2000 wing/flap configuration will be discussed. In section 3.4.1 the effect of sandpaper roughness at the leading edge is studied. The calculations have been done for the retracted wing/flap geometry. The results are compared with flight test data. In section 3.4.2 the roughness model has been used to simulate the effect of a de-icing fluid covering the wing and the flap.

3.3.1 Sand paper roughness at leading edge

In this section the effect of sandpaper roughness at the leading edge is studied. For the

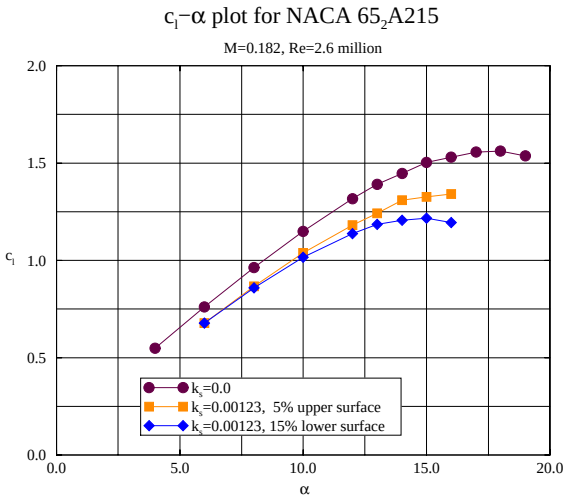

Fig. 5 Computed c_l for NACA $65_2 - A215$ at M_∞=0.182, Re=2.6 million and different values on the roughness parameter k_s.

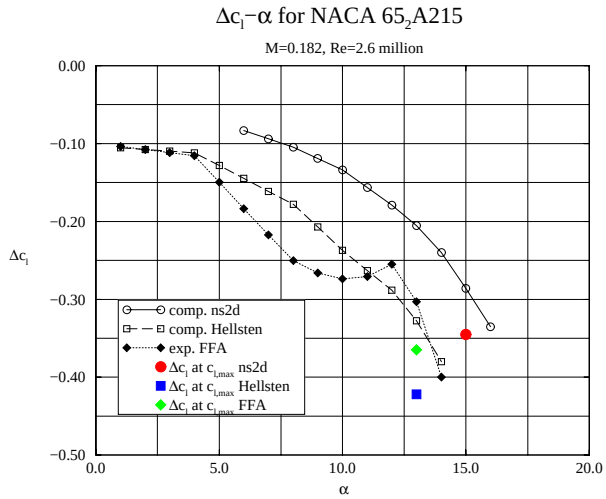

Fig. 7 Δc_l versus α for NACA $65_2 - A215$ at M_∞=0.182 and Re=2.6 million.

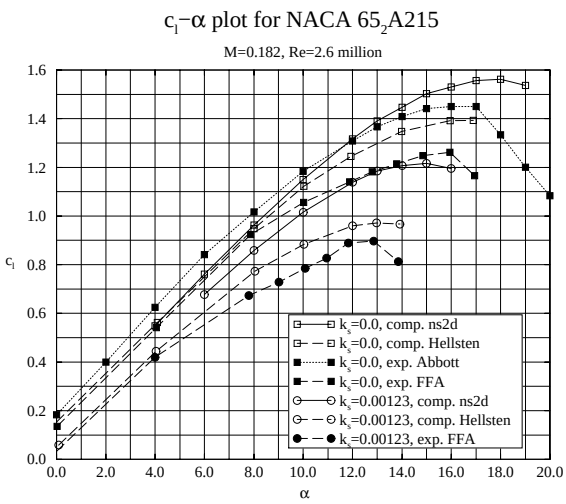

Fig. 6 Comparison between measured and computed c_l for NACA $65_2 - A215$ at M_∞=0.182 and Re=2.6 million. (Remark: In Abbott Re=3.0 million was used).

chosen test cases there are flight test data available. All calculations have been done for the retracted wing/flap geometry at a free stream Mach number of M_∞=0.18 and Reynolds number of Re=11.2 million. In the flight test setup a sand paper roughness of 300 microns was chosen. This corresponds to k_s/c=0.0002. The wing/flap geometry used in the present 2D calculations was obtained from the wing cross section at 1.7 m from the wing root section. Following the experimental setup 0.4% of lower side and 1.1% of the upper was covered by sand roughness. The leading edge roughness results in a decrease of the suction peak, in the c_p-distribution, which in turn leads to a lower c_l. In figure 8 the lift curves for the clean and rough airfoil are displayed. Corresponding results from flight tests are found in figure 9. Even if the absolute values of c_l are not exactly the same, the Δc_l, i.e. the losses in c_l between clean and rough airfoil, agree rather well as can be seen in figure 10.

3.3.2 De-icing fluid roughness

The main objective of the present work was to estimate the lift losses due to deicing fluids which partially cover the wing and flap. Both retracted flap, $\delta_f = 0^o$, and flap at flap position $\delta_f = 15^o$ have been considered. Different values of the

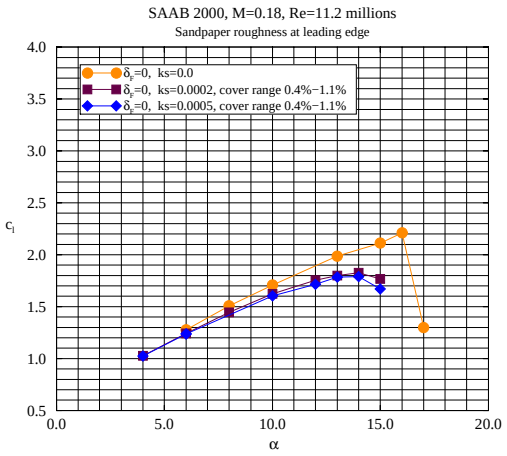

Fig. 8 Computed $c_l - \alpha$ curves showing the effect of leading edge roughness on the SAAB 2000 wing with retracted flap, M_∞=0.18 and Re=11.2 million.

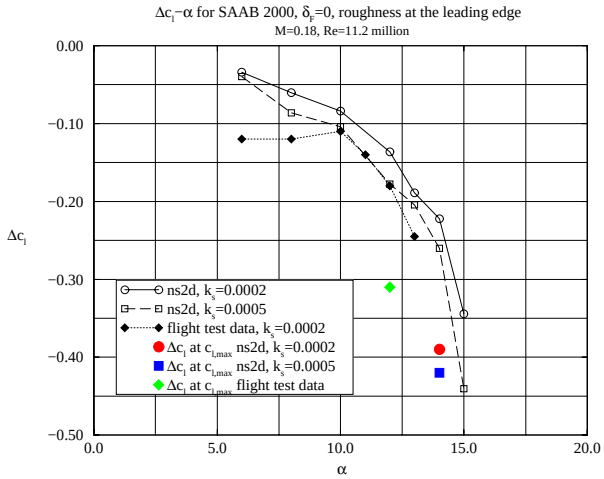

Fig. 10 Δc_l versus α for SAAB 2000 wing with retracted flap and leading edge roughness, M_∞=0.18 and Re=11.2 million. (Remark: the calculations are 2D and flight tests 3D).

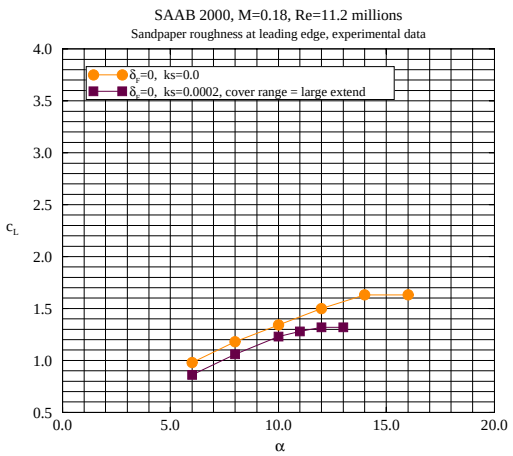

Fig. 9 Flight test $c_l - \alpha$ curves showing the effect of leading edge roughness on the SAAB 2000 wing with retracted flap, M_∞=0.18 and Re=11.2 million.

roughness parameter k_s and the cover range have been studied. We will first discuss the results for the retracted flap, $\delta_f = 0^o$. A free stream Mach number of M_∞=0.18 and Reynolds number of Re=11.2 million were chosen. The calculations were done for four values of the roughness parameter k_s, (0, 0.0005, 0.0010 and 0.0015) and the cover range was 10%-100% of the upper part of the wing surface. For all calculations the angle of attack α varies from 6° up to 17° which is beyond $\alpha_{c_{l,max}}$. As can be seen in figure 11 the pressure curve becomes more flat at high angles of attack α indicating flow separation at the rear part of the wing. Also the suction peak decreases. The lift curves for both smooth and rough surfaces are shown in figure 12.

For the rough cases, calculations beyond $\alpha_{c_{l,max}}$ have also been performed. The results are however uncertain, due to the unsteadiness of the flow, and have hence been omitted in figure 12. For comparison a calculation with k_s=0.0010 and the cover range 40%-100% was also performed. The plot in figure 14 shows how the increase of the displacement thickness effects the c_l losses. The displacement thickness was evaluated at 80% of the chord. The computed data,

which include different values of k_s and the cover range, are clustered around a straight line. Similar results were presented by Fokker at the ERA meeting 1995 (ref. [1]).

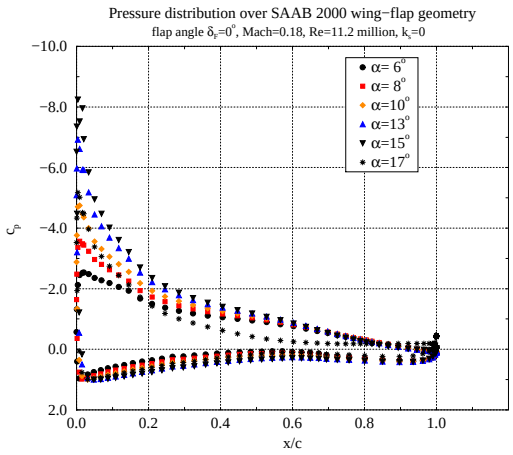

Fig. 11 Pressure distribution, for different angles of attack α, over SAAB 2000 wing with retracted flap, M_∞=0.18, Re=11.2 million and k_s=0.

We will finally look at the computed results for SAAB 2000 wing/flap configuration for $\delta_f = 15^o$. The same flow conditions as above have been applied. Four selections of surface roughness were used k_s=0/0, 0.0005/0.0025, 0.0010/0.0025, 0.0005/0.0005 where */* denotes the roughness of the wing/flap. The roughness cover range was the same as for $\delta_f = 0^o$ for the wing. On the flap 23%-100% of the upper surface was covered. Since a collection of de-icing fluids can be expected on the flap, a higher k_s was chosen for the flap than for the wing. In figure 15 the pressure distributions over the wing/flap are displayed. The same observations and conclusions, concerning the pressure distribution, which were drawn for $\delta_f = 0^o$ are also valid in this case.

The effects of surface roughness on the lift coefficient can be seen in figure 16. We observe from this plot that the effect of roughness is more pronounced compared to that for $\delta_f = 0^o$. Typically the lift losses at $\alpha_{c_{l,max}}$ are 0.16-0.30 for

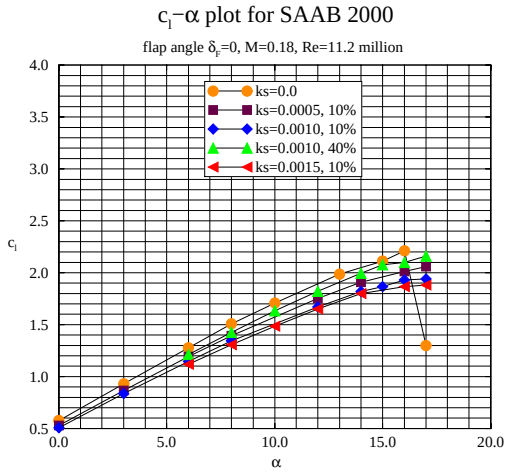

Fig. 12 The effect of surface roughness on the $c_l - \alpha$ curve for the SAAB 2000 wing with retracted flap.

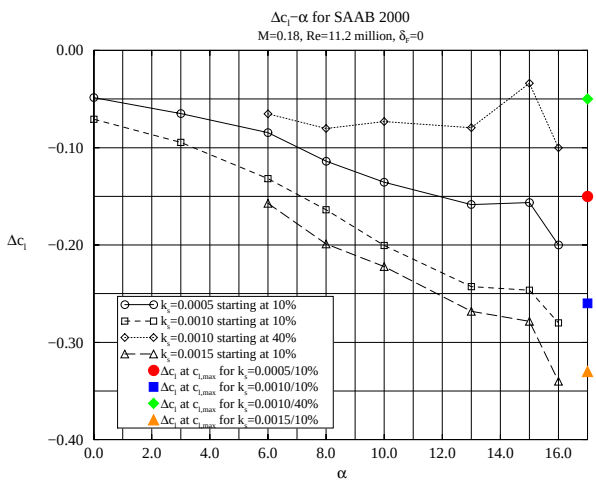

Fig. 13 Δc_l versus α at different surface roughness for the SAAB 2000 wing with retracted flap, M_∞=0.18 and Re=11.2 million.

$\delta_f = 0^o$ whereas lift losses of 0.36-0.69 are obtained for $\delta_f = 15^o$. From the lift curve we also observe a shift in $\alpha_{c_{l,max}}$ for k_s>0. It should be

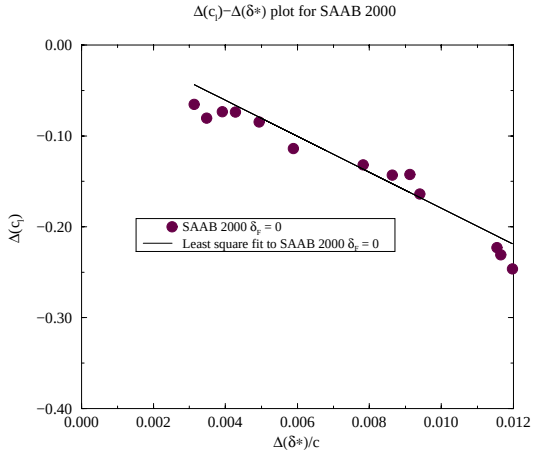

Fig. 14 Lift losses versus the change of the displacement thickness for SAAB 2000 wing with retracted flap, M_∞=0.18 and Re=11.2 million.

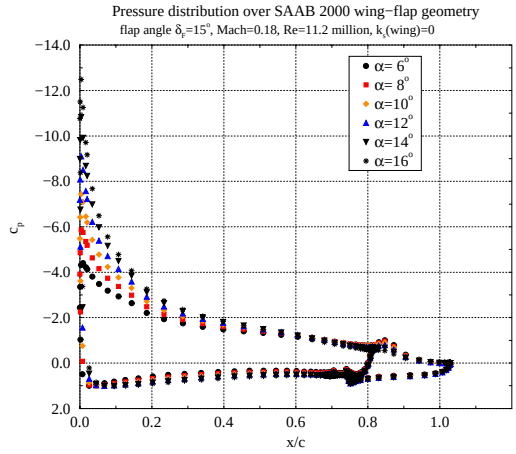

Fig. 15 Pressure distribution, for different angles of attack, over the SAAB 2000 wing at flap angle $\delta_f = 15^o$, M_∞=0.18, Re=11.2 million and k_s=0.

mentioned that for $\delta_f = 15^o$ unsteadiness in the flow field was observed for all flow cases. Hence a time average has been used when computing c_l, Δc_l.

Figure 18 finally shows how the increase of the displacement thickness effects the loss of c_l. The computed data, which include different values of k_s and the cover range, are clustered around a straight line in the same way as in the previous calculations. The slope of the line is however slightly steeper, compare to that of $\delta_f = 0^o$, indicating a higher sensitivity to changes of the boundary layer thickness.

3.4 Summary and conclusion

In the present paper the effect of surface roughness on a flow field has been studied by means of the 2D Navier-Stokes code ns2d. The Chien's $\kappa - \varepsilon$ model has been used to model the turbulence. The roughness is taken into account through a modification of the wall distance. Several test cases have been used to validate the code. For some of them comparisons with wind tunnel and flight test data have been performed.

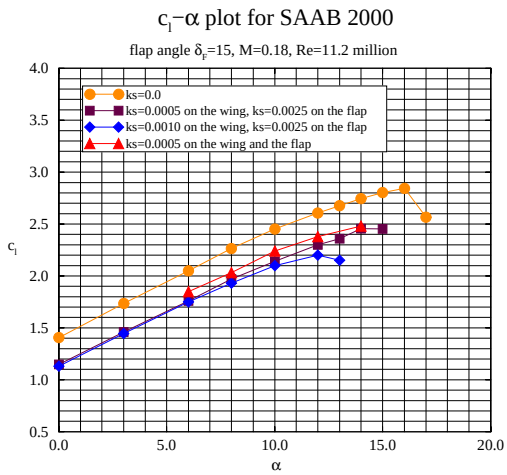

Fig. 16 Effect of surface roughness on the $c_l - \alpha$ curve for the SAAB 2000 wing at flap angle $\delta_f = 15^o$, M_∞=0.18 and Re=11.2 million.

The main part of the computations have been focused on the SAAB 2000 wing flap configuration. The effect of both leading edge roughness

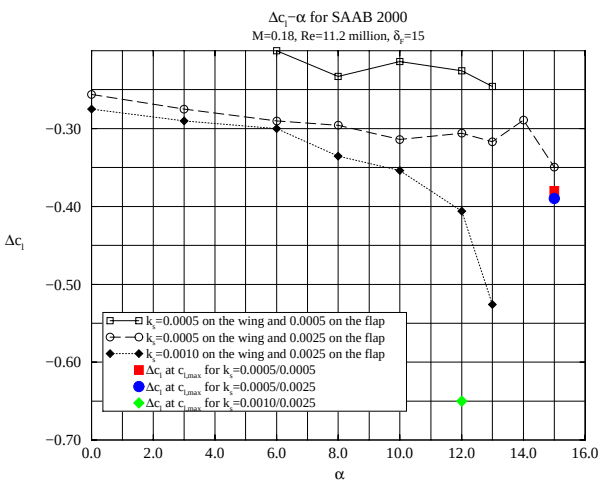

Fig. 17 Δc_l versus α at different surface roughness for SAAB the 2000 wing at flap angle $\delta_f = 15^o$, M_∞=0.18 and Re=11.2 million.

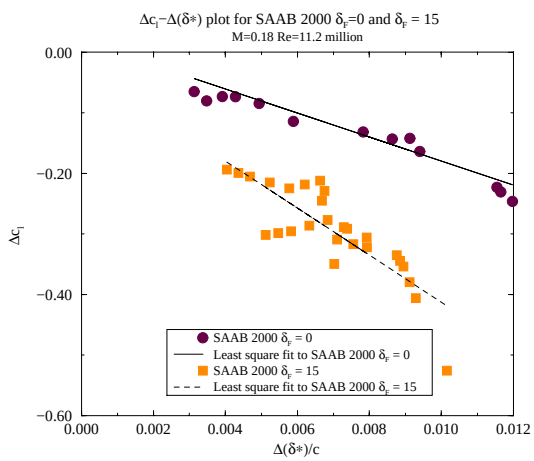

Fig. 18 Lift losses versus changes in displacement thickness (at 80% of the chord) at varying surface roughness for SAAB 2000 wing/flap configuration at flap angle $\delta_f = 0^o$ and $\delta_f = 15^o$.

and de-icing fluid roughness have been studied. In the first case lift losses of the same magnitude as from flight tests were computed. In the second case typical losses in c_l, for a retracted wing/flap configuration and a surface roughness in the range k_s=0.0005-0.0010, of 0.1 were predicted for low α. For α close to $\alpha_{c_{l.max}}$ losses of 0.16-0.30 were observed. For a flap angle of $\delta_f = 15^o$ higher lift losses, around 0.3 for low α and 0.36-0.69 at $\alpha_{c_{l.max}}$ were found.

References

[1] Fokker. Ground anti-de-icing fluids. *ERA Meeting Amsterdam*, 2 September, 1995.

[2] Hellsten A and Laine S. Extension of the $\kappa - \omega$ -sst turbulence model for flows over rough surfaces. *AIAA paper 97-3577*, 1997.

[3] Larsson T. Separated and high-lift flows over single and multi-element airfoils. *ICAS paper 94-5.7.3*, 1994.

[4] Lee J. Modeling boundary layer flows over rough surfaces using a modified chien $\kappa - \varepsilon$ turbulence model. *AIAA paper 96-0384*, 1996.

[5] Ljungström B. L. Wind tunnel investigation of simulated hoar frost on a 2d wing section with and without high lift devices. *Report FFA AU-902, The Aeronautical Research Institute of Sweden*, 1972.

[6] Rotta J. Turbulent boundary layers in incompressible flow. *Progress in Aeronautical Sciences, Pergammon Press, N.Y.*, Vol. 2, 1962.

[7] SAAB. Leading edge roughness on saab 2000, flight test data. *SAAB Report 73ADS0135*.

[8] Schlichting. *Boundary Layer Theory*. McGraw-Hill, 1960.